JACS
JOURNAL OF THE AMERICAN CHEMICAL SOCIETY
Article
Cite This: J. Am. Chem. Soc. 2018, 140, 14952−14957
pubs.acs.org/JACS

Ultrafast Broadband Charge Collection from Clean Graphene/$CH_3NH_3PbI_3$ Interface

Hao Hong,[†,○] Jincan Zhang,[‡,○] Jin Zhang,[§,○] Ruixi Qiao,[†] Fengrui Yao,[†] Yang Cheng,[†] Chunchun Wu,[∥] Li Lin,[‡] Kaicheng Jia,[‡] Yicheng Zhao,[†] Qing Zhao,[†] Peng Gao,[⊥] Jie Xiong,[∥] Kebin Shi,[†] Dapeng Yu,[#,▽] Zhongfan Liu,[‡] Sheng Meng,[*,§] Hailin Peng,[*,‡] and Kaihui Liu[*,†]

[†]State Key Laboratory for Mesoscopic Physics, Collaborative Innovation Centre of Quantum Matter, School of Physics, Peking University, Beijing 100871, China

[‡]Center for Nanochemistry, College of Chemistry and Molecular Engineering, Academy for Advanced Interdisciplinary Studies, Peking University, Beijing 100871, China

[§]Beijing National Laboratory for Condensed Matter Physics, Institute of Physics, Chinese Academy of Sciences, Beijing 100190, China

[∥]State Key Laboratory of Electronic Thin Films and Integrated Devices, University of Electronic Science and Technology of China, Chengdu 610054, China

[⊥]International Centre for Quantum Materials, Peking University, Beijing 100871, China

[#]Institute for Quantum Science and Engineering and Department of Physics, South University of Science and Technology of China, Shenzhen 518055, China

[▽]Shenzhen Key Laboratory of Quantum Science and Engineering, Shenzhen 518055, China

Supporting Information

ABSTRACT: Photocarrier generation in a material, transportation to the material surface, and collection at the electrode interface are of paramount importance in any optoelectronic and photovoltaic device. In the last collection process, ideal performance comprises ultrafast charge collection to enhance current conversion efficiency and broadband collection to enhance energy conversion efficiency. Here, for the first time, we demonstrate ultrafast broadband charge collection achieved simultaneously at the clean graphene/organic−inorganic halide perovskite interface. The clean interface is realized by directly growing perovskite on graphene surface without polymer contamination. The tunable two-color pump−probe spectroscopy, time-resolved photoluminescence spectroscopy, and time-dependent density functional theory all reveal that the clean-interfacial graphene collects band-edge photocarriers of perovskite in an ultrashort time of ∼100 fs, with a current collection efficiency close to 99%. In addition, graphene can extract deep-band hot carriers of perovskite within only ∼50 fs, several orders faster than hot carrier relaxation and cooling in perovskite itself, due to the unique Dirac linear band structure of graphene, indicating a potential high energy conversion efficiency exceeding the Shockley−Queisser limit. Adding other graphene superiority of good transparency, high carrier mobility, and extreme flexibility, clean-interfacial graphene provides an ideal charge collection layer and electrode candidate for future optoelectronic and photovoltaic applications in two dimensions.

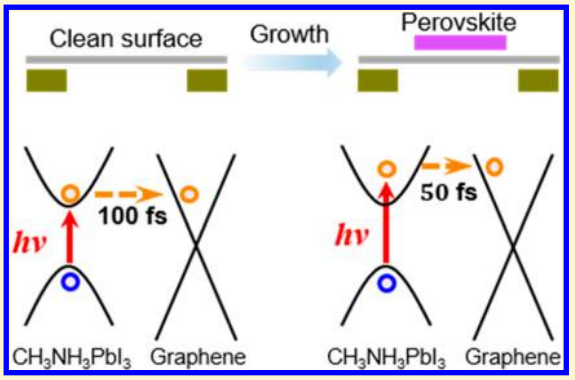

INTRODUCTION

In all optoelectronic and photovoltaic devices, three essential processes are involved to accomplish photocurrent generation or photoenergy harvesting: light absorption in a material to generate photocarriers, photocarrier transportation to the material surface, and charge collection to the electrode. The engineering and optimization of these three processes lie at the center of improving the photoelectric device performance. The emergent absorber materials of organic−inorganic halide perovskites (e.g., $CH_3NH_3PbI_3$) shed bright light on optimizing the first two key photoelectric processes, as this family of materials have a tunable bandgap from visible to near-infrared with high absorption coefficient (over 10^4 cm^{-1} above bandgap) to ensure high photocarrier generation efficiency,[1] strong dielectric screening with negligible exciton binding energy (<25 meV at room temperature) to facilitate electron hole separation,[2,3] and long carrier diffusion length (up to sub millimeter) to render the effective carrier transportation to the material surface.[4−8]

Received: August 30, 2018
Published: October 15, 2018

DOI: 10.1021/jacs.8b09353
J. Am. Chem. Soc. 2018, 140, 14952−14957

The searching for new materials and controlling the interface for effective charge collection remain as the bottleneck challenges to further improve the photoelectric conversion efficiency in these emergent absorber materials. In principle, an ideal charge collection comprises two features: (i) ultrafast charge collection to enhance current conversion efficiency and (ii) broadband collection including hot carriers to enhance energy conversion efficiency. Although the physical picture is quite clear,[9−13] conventional collection layers, such as TiO_2, Spiro-OMeTAD, or PCBM, do not fully satisfy the above two requirements,[14−18] possibly due to nonideal material properties, poor band alignment, and low interfacial coupling quality. Therefore, searching for effective carrier collection materials with proper properties and fabricating high-quality interfaces are essential to further improve the performance of photoelectric devices.

The rise of two-dimensional (2D) materials provides new opportunities for efficient charge collection, due to the highly tunable and distinct physical properties compared to their bulk counterparts.[19,20] Examples include fully exposed electronic states at surface facilitating strong interfacial electronic hybridization and coupling,[21−23] and superflat surface without dangling bond enabling clean interface and high-quality van der Waals epitaxial growth.[24−26] Graphene, the representative 2D material, features high carrier mobility, extreme flexibility, good optical transparency, and chemical inertness and thus performs as the best electrode in two dimensions.[27−30] Most importantly, graphene has Dirac linear electronic bands with broadband photoresponse from 0 to ∼6 eV,[31] a unique property potentially enabling hot carrier collection under broadband excitation energies. Indeed, graphene electrode has demonstrated superior photoelectric performance, ranging from energy-efficient electronic switches,[32] THz photoresponse rate in vertical heterostructures,[33,34] and high performance hybrid photodetector[35−38] to largely enhanced efficiency in solar cells.[39,40] However, comprehensive and quantitative understanding of the photoelectric performance of graphene as a charge collection material at femtosecond time scale with accurate interfacial control is still rare and at its very early stage.

In this article, we demonstrate the first ultrafast broadband charge collection from clean graphene/$CH_3NH_3PbI_3$ (Gr/$MAPbI_3$) interface, which is realized by a polymer-free transfer of chemical vapor deposition (CVD) grown graphene film and the direct growth of $MAPbI_3$ on clean graphene surface. Our ultrafast optical spectroscopy and time-dependent density functional theory (TDDFT) all reveal that the clean-interfacial graphene will collect band-edge photocarriers of $MAPbI_3$ in an ultrashort time of ∼100 fs with a current collection efficiency close to 99%. In addition, graphene can extract deep-band hot carriers of $MAPbI_3$ within only ∼50 fs (orders of magnitude faster than hot carrier relaxation and cooling in $MAPbI_3$ itself), indicating potential high energy conversion efficiency exceeding Shockley−Queisser limit. These above superior photocarrier collection properties are attributed to the clean Gr/$MAPbI_3$ interface and graphene's unique Dirac linear band structure. Our work provides a concrete proof of concept that clean-interfacial graphene is an effective planner charge collection material for high performance optoelectronic and photovoltaic applications with potential high current and energy conversion efficiency in two dimensions.

RESULTS

Gr/$MAPbI_3$ Heterostructure with Clean Interface. Clean interface between graphene and $MAPbI_3$ was realized by combining our polymer-free graphene transfer technique with the direct $MAPbI_3$ growth method.[41,42] Graphene film was grown by CVD on the surface of catalytic Cu foil. Suspended graphene on a transmission electron microscopy (TEM) grid was prepared using the nonpolymer-assisted clean transfer method (Figure 1a). This procedure perfectly avoids polymer contamination during transfer and exposes the clean graphene surface that is originally adhered to and protected by Cu. Then, contacting perovskite single crystals were directly synthesized on the clean graphene surface using a one-step solution process with a thickness of 5−100 nm. As shown in the TEM image (Figure 1b), $MAPbI_3$ crystal with regular rectangular shape and uniform thickness (∼10 nm) resides on the suspended graphene surface. Meanwhile, there were no noticeable contaminants observed around the graphene/$MAPbI_3$ area.[42] The aberration-corrected atomic-resolved TEM images and corresponding fast Fourier transform (FFT) images of graphene (Figure 1c) and $MAPbI_3$ (Figure 1d) further prove their high crystallinity. In addition, no detectable D peaks (disorder related peak) were observed in Raman spectra of graphene before and after perovskite growth, indicating the high quality of the graphene film (Figure 1e). By carefully reviewing the quantitative shifts of G and 2D peaks of graphene before and after $MAPbI_3$ growth, we can deduce that the growth of $MAPbI_3$ induces within ∼0.1% tensile strain to graphene lattice and also slightly dopes graphene due to graphene-$MAPbI_3$ coupling.[43] This coupling effect can be also observed in the photoluminescence (PL) spectra of pristine $MAPbI_3$ and Gr/$MAPbI_3$, where $MAPbI_3$'s PL intensity was quenched by nearly two orders of magnitude in the hybrid structure (Figure 1f).

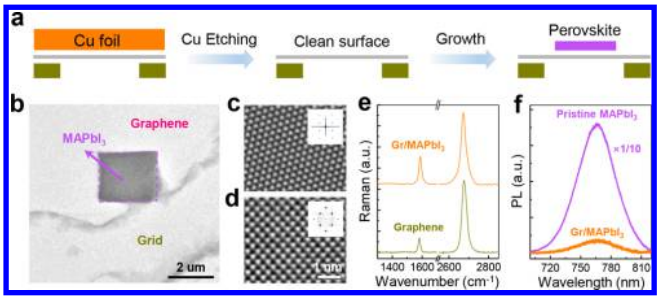

Figure 1. Fabrication, structure, and properties of Gr/$MAPbI_3$ heterostructure with clean interface. (a) Fabrication scheme of clean-interfacial Gr/$MAPbI_3$ heterostructure, including the steps of adhering graphene to a holey substrate, etching Cu substrate to uncover the clean graphene surface, and one-step solution growing $MAPbI_3$ single crystals on the clean graphene surface. (b) TEM image of the suspended Gr/$MAPbI_3$. (c,d) Representative aberration-corrected TEM images of graphene (c) and $MAPbI_3$ (d), displaying the perfect lattice structure without contamination and defects. Insets correspond to the fast Fourier transform of the HRTEM images. (e) Raman spectra of graphene before and after $MAPbI_3$ growth. (f) Photoluminescence spectra of $MAPbI_3$ with and without graphene beneath.

Ultrafast Band-Edge Charge Collection Dynamics at Clean Gr/$MAPbI_3$ Interface. To capture the ultrafast charge collection dynamics at band edge, we applied ultrafast tunable two-color pump−probe spectroscopic measurement to the Gr/

DOI: 10.1021/jacs.8b09353
J. Am. Chem. Soc. 2018, 140, 14952−14957

$MAPbI_3$ structure. We pump $MAPbI_3$ band edge by 820 nm pulse (width of ~100 fs, fluence of 1.3 $\mu J/cm^2$) and probe the possible charge collection signal by a shorter wavelength at 620−720 nm (Figure 2a). This longer-wavelength pump and shorter-wavelength probe technique can largely avoid the signal detection of individual $MAPbI_3$ and graphene themselves but selectively detect the signal from the charge collection at the interface (Figure S1).[44,45] The probe wavelength-dependent transient absorption signal at different pump−probe delay time is shown in the 2D mapping (Figure 2b). The horizontal cut of the 2D mapping gives out the wavelength dependence and a peak around 680 nm, which reflects the band offset of ~0.6 eV between valence band edge of $MAPbI_3$ and charge neutral point of graphene (Figure S2). The vertical cut of the 2D mapping (Figure 2c) reveals the charge collection dynamics at interface (rising-up part) and following carrier relaxation in graphene (decaying-down part). Zoom-in rising-up curve (Figure 2d) reveals obviously that charge collection at clean-interfacial Gr/$MAPbI_3$ is within ultrashort time scale of ~100 fs. In sharp contrast, at the dirty-interfacial Gr/$MAPbI_3$ (containing considerable polymer contaminations during the polymer-assisted transfer process of graphene), the charge collection time (~530 fs) is five times longer.

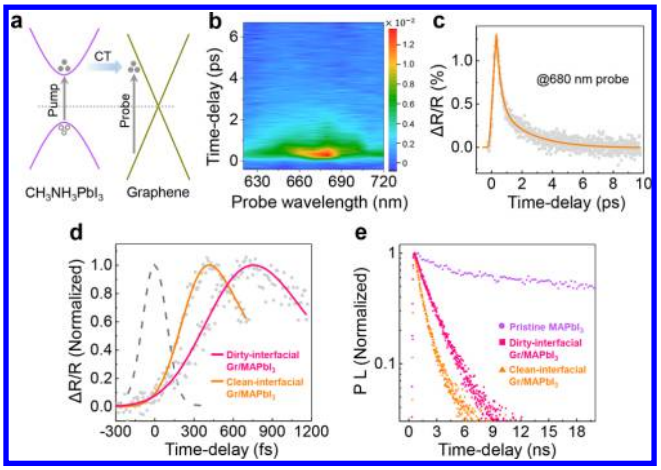

Figure 2. Ultrafast band-edge charge collection at clean Gr/$MAPbI_3$ interface. (a) Scheme of band alignment and the band-edge charge collection of graphene from $MAPbI_3$. (b) Two-dimensional plots of transient absorption signal of clean-interfacial Gr/$MAPbI_3$ at different probe wavelength with pump wavelength of 820 nm. (c) Evolution of transient absorption signal with probe wavelength at 680 nm. The selected trace undergoes biexponential decay with lifetime of 0.3 and 2.1 ps, representative dynamics from graphene. (d) By deconvolution of the rising-up transient absorption signal based on laser cross-correlation function (dash line), the charge collection time for clean-interfacial Gr/$MAPbI_3$ is determined to be ~100 fs, but ~530 fs for polymer-contaminated one. (e) Time-resolved photoluminescence of pristine $MAPbI_3$, $MAPbI_3$ grown on polymer-contaminated graphene, and clean graphene measured, with lifetime of 79.0, 1.8, and 1.0 ns, respectively.

Ultrafast charge collection will greatly facilitate the high current conversion efficiency. Under the ~100 fs ultrafast charge transfer process, the collection efficiency will be very close to 100% at the interface, while in reality photocarriers have the chance to be trapped by defect states in the body or at the surface[46] and cannot diffuse to the interface immediately. To quantitative estimate the actual charge collection efficiency in our heterostructures, we carried out time-resolved photoluminescence spectroscopy (TRPL) to obtain the photocarrier recombination lifetime in pristine $MAPbI_3$ and Gr/$MAPbI_3$ with clean and dirty interfaces (Figure 2e). Pristine $MAPbI_3$ has lifetime τ_0 of ~79.0 ns, while in clean-interfacial structure the lifetime τ_1 reduced significantly to ~1.0 ns. By using the relation $\left(\eta = 1 - {}^{\tau_1}/_{\tau_0}\right)$,[14] charge collection efficiency η in the clean-interfacial structures can be estimated as high as 98.7%, closing to the ideal limit. In contrast, the $MAPbI_3$ grown on polymer-contaminated graphene gives out lifetime τ_1' of ~1.8 ns, 80% longer than the clean-interfacial one. We note here, even in the dirty-interfacial Gr/$MAPbI_3$ structure, the estimated charge collection efficiency is still not low (97.7%), due to the superior intrinsic ultralong carrier lifetime in pristine $MAPbI_3$. However, in general, for absorber materials with a picosecond time scale carrier lifetime, the collection efficiency difference between clean and dirty interfaces will be significant.

Ultrafast Deep-Band Hot Carrier Collection at Clean Gr/$MAPbI_3$ Interface. A great concern in charge collection is whether the hot carrier in deep band can be harvested or not, which is the key to enhance the energy conversion efficiency. The relative cooling dynamic lifetime in $MAPbI_3$ itself and the interfacial charge collection process in deep band determine the hot carrier collection efficiency. According to our TRPL result (Figure S3), the hot carrier relaxation and cooling will take ~50 ps at room temperature, accompanied by strong electron-defect, electron−electron, and electron−phonon scattering. In conventional charge collection materials, such as TiO_2, Spiro-OMeTAD, PCBM, etc., the collection lifetime is

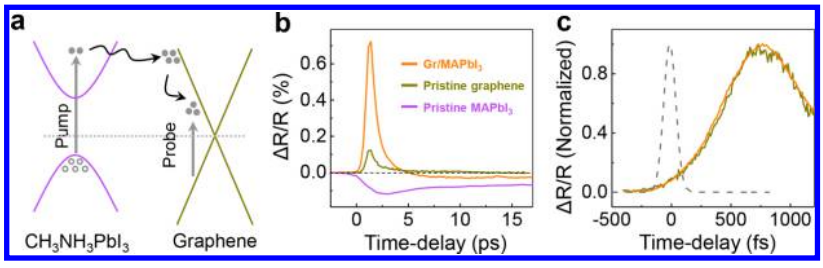

Figure 3. Ultrafast deep-band hot carrier collection at clean Gr/$MAPbI_3$ interface. (a) Scheme of band alignment and the deep-band charge collection of graphene from $MAPbI_3$ under optical excitation of larger photon energy. (b) Evolution of transient absorption signal of pristine $MAPbI_3$, pristine graphene, and clean-interfacial Gr/$MAPbI_3$. The signal of Gr/$MAPbI_3$ features both pristine $MAPbI_3$ and graphene, except the graphene signal part is strongly enhanced while $MAPbI_3$ part is depressed, revealing the hot carrier transfer from $MAPbI_3$ to graphene. (c) Comparison of the rising-up curve of Gr/$MAPbI_3$ and pristine graphene. The same trend reveals the hot carrier collection is ultrafast below our setup resolution (~50 fs).

DOI: 10.1021/jacs.8b09353
J. Am. Chem. Soc. 2018, 140, 14952−14957

in the order of few tens of picoseconds; therefore, these materials cannot collect deep-band hot carriers efficiently.

To verify if clean-interfacial graphene can be a good hot carrier collector, we carried out shorter-wavelength pump and longer-wavelength probe spectroscopy to investigate the interfacial charge collection at deep band of Gr/$MAPbI_3$ (Figure 3a). We generate the deep-band photoelectrons in $MAPbI_3$ by 400 nm pump pulse laser (width of ~70 fs, fluence of 4.1 $\mu J/cm^2$) and probe the hot carriers that transferred to graphene by a selective wavelength of 690 nm. This probe wavelength is purposely chosen as 75 nm longer than the $MAPbI_3$ bandgap wavelength, which can largely decrease the strong bleaching signal in $MAPbI_3$ itself.

Time-resolved transient absorption signals of Gr/$MAPbI_3$, pristine graphene, and $MAPbI_3$ were shown in Figure 3b. For pristine graphene or $MAPbI_3$, the dynamic curve is consistent with previous results and understanding.[14,47] In graphene, transient absorption signal will quickly rise up within ~1 ps and then decay to zero in the next few picoseconds, while in $MAPbI_3$, a negative transient absorption signal shows up at ~2.5 ps (hot carrier relaxation,τ_{relax}) and then relaxes to zero in the next nanosecond time scale.

In Gr/$MAPbI_3$, the decaying-down behavior is a combination of pristine graphene and $MAPbI_3$, where transient absorption signal first decays in several picoseconds, evolves from positive to negative, and then relaxes in nanoseconds, while the rising-up curve reflects the charge transfer characteristics. Two features unambiguously reveal the hot carrier collection of graphene from $MAPbI_3$. First, the amplitude of rising-up signal is six times larger than the pristine graphene (Figure 3b), which is induced by the charge collected from $MAPbI_3$; second, the speed of the rising-up curve is the same as in the pristine graphene (Figure 3c), which indicates that charge collection time scale is already less than our experiment resolution (τ_{CT}) of ~50 fs. We estimate the hot carrier collection efficiency from the charge collection lifetime and hot carrier relaxation time $\left(\eta = 1 - {}^{\tau_{CT}}/_{\tau_{relax}}\right)$ as 98% at the interface, which means a very high efficiency.

Time-Dependent Density Function Calculations of Interfacial Charge Collection Dynamics. We choose a large supercell for $MAPbI_3$ (168 atoms) and graphene (120 atoms) to start the TDDFT calculation[48−50] and monitored the charge distribution in graphene and $MAPbI_3$ at different time after photoexcitation (see details in Note S1). It is clear that the photocarriers can almost fully transfer to graphene within 400 fs (Figure 4a). To track the photoexcitation-induced electron dynamics more quantitatively, we performed nonadiabatic molecular dynamics and monitored the integrated electron population on the graphene orbitals at different time after photoexcitation. For band-edge excitation in $MAPbI_3$, the charge collection time is fitted as ~90 fs (Figure 4b), and for deep-band excitation (~3.0 eV) in $MAPbI_3$, the charge collection time is ~30 fs (Figure 4c). These simulation results are well consistent with our experimental observation that clean-interfacial graphene can collect both cooling carriers and hot carriers in an ultrafast way with a very broad spectrum from the band edge of 1.5 eV to deep band of 3.0 eV (Figure 4d). The clean interface is critical to realize the ultrafast charge collection in Gr/$MAPbI_3$ because it is essential to ensure strong interfacial coupling. In the dirty interface, where the interfacial distance can be increased by few angstroms, the charge collection time elongates to a much longer time scale since the interlayer coupling evolves obviously with interlayer distance.[22]

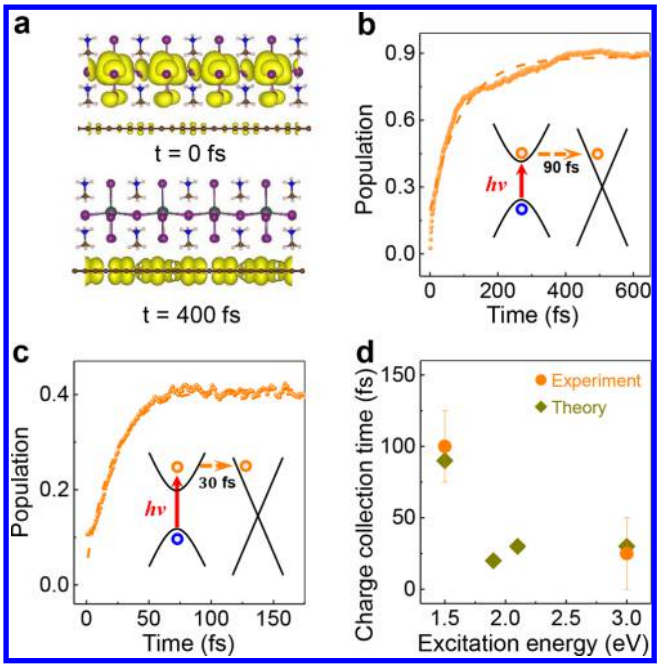

Figure 4. Time-dependent density function calculations of interfacial charge collection dynamics of Gr/$MAPbI_3$. (a) Electron population distributions at t = 0 fs (upper panel) and t = 400 fs (lower panel), after the initial band-edge photoexcitation of Gr/$MAPbI_3$ heterostructure. (b) Evolution of integrated electron population on the graphene orbitals under different time after band-edge photoexcitation. The charge collection time is fitted to ~90 fs. (c) For a deep-band excitation with photoenergy of 3.0 eV, the hot carrier collection is also ultrafast, with fitted charge collection time of ~30 fs. (d) From calculation and experiment, the charge collection of $MAPbI_3$ by clean graphene electrode is ultrafast within a very wide spectral range, indicating the potential high energy conversion efficiency.

DISCUSSION

The superior photocarrier collection performance of graphene is the consequence of its unique properties. First, it has saturated π bonds at the surface and can facilitate the superclean interface with the 2D absorber materials; second, it has Dirac linear band structure that can ensure broadband charge collection including deep-band hot carriers as well. In addition, graphene can act as charge collection material and conducting electrode at the same time, which can avoid the further charge and energy consumption during the transportation between them. Considering graphene's other superiority of good transparency, high carrier mobility, and extreme flexibility, clean-interfacial graphene is very competitive as efficient charge collection material in two dimensions. Recently, 2D perovskite system develops rapidly and performs pleasing physical properties, such as photo/chemical stability,[51,52] tunable optoelectronic properties,[53] peculiar edge states,[46] and so on. In most of these studies, gold is used as the electrode (our control experiment shows that the charge collection efficiency in the gold electrode system is far below graphene). The combination of graphene electrode engineering with 2D perovskite material engineering will likely lead to significant efficiency improvement of photoelectric conversion soon.

DOI: 10.1021/jacs.8b09353
J. Am. Chem. Soc. 2018, 140, 14952−14957

In the future, to apply clean-interfacial graphene into real optoelectronic and photovoltaic applications, the challenge still remains as graphene can collect both electrons and holes, and they may combine in graphene itself before being extracted to the external circuit. This challenge in principle can be conquered by band filling control through external electric/magnetic field,[54,55] adhering exotic layers on the other graphene side.[56,57] The massive production of single-crystal graphene and clean-surface graphene transfer technique is readily available now,[58,59] and the high performance optoelectronic and photovoltaic devices based on clean-interfacial graphene are awaiting.

METHODS

Sample Preparation and TEM Characterization. Large single-crystal graphene was grown on Cu foil (Alfa-Aesar, No. 46365) by chemical vapor deposition method. Polymer-free transfer technique is applied to fabricate suspended graphene with clean surface.[42] For $MAPbI_3$ synthesis, CH_3NH_3I and PbI_2 were dissolved in isopropanol at a 3:1 molar ratio with solution concentration of ∼40%. Then, the graphene grid was floated on the surface of perovskite solution with the clean graphene face contacting the solution instead of rinsing it in the solution. Aberration-corrected-TEM experiments were performed in a JEOL ARM 3000 under 80 kV with low electron dose to minimize the beam damage. The diffraction patterns were obtained by a FEI TECNAI F20 operated at 200 kV.

Transient Absorption Spectrum. Femtosecond pulses (∼100 fs, 80 MHz) at 820 nm are generated by a Ti:sapphire oscillator (Spectra-Physics Mai Tai laser). The diameters of focused pump and probe pulse are about 2 and 1 μm, respectively. This laser was used in the band-edge charge collection measurement. In the deep-band charge collection measurement, the laser source was replaced by a lower repetition rate pulse laser (Coherent laser, 250 kHz, ∼70 fs), as the lifetime of $MAPbI_3$ is much longer than the time interval of Mai Tai laser pulses. The TA signal, $\Delta R/R = (R_{\text{with pump}} - R_{\text{without pump}})/R_{\text{without pump}}$, was recorded by a PMT and lock-in amplifier with reflective geometry. The experimental scheme is shown in our previous work.[45] In all experiments, the pump fluence is quite low to avoid involving nonlinear processes (Figure S4).

Time-Resolved Photoluminescence. Two pulse laser sources were alternatively used in TRPL measurement, i.e., 410 nm with 80 MHz repetition rate and 400 nm with 250 kHz repetition rate. After photoexcitation and collection, the PL signal of target wavelength was selected by a 460 long-pass filter and a spectrometer (resolution of ±2 nm). Then, we used single-photon avalanche photodiode detector (PicoQuant Company, TDA 200) combining with a time-correlated single photon counting module (TimeHarp 260 PICO Single) to obtain the time-resolved TRPL signal.

ASSOCIATED CONTENT

Supporting Information

The Supporting Information is available free of charge on the ACS Publications website at DOI: 10.1021/jacs.8b09353.

Transient absorption signal of pristine graphene and $MAPbI_3$, band alignment determination, $MAPbI_3$ hot carrier relaxation and cooling, linear transient absorption, and methods for TDDFT (PDF)

AUTHOR INFORMATION

Corresponding Authors

*khliu@pku.edu.cn
*hlpeng@pku.edu.cn
*smeng@iphy.ac.cn

ORCID

Jin Zhang: 0000-0001-7830-3464
Qing Zhao: 0000-0003-3374-6901
Peng Gao: 0000-0003-0860-5525
Jie Xiong: 0000-0003-3881-6948
Zhongfan Liu: 0000-0003-0065-7988
Sheng Meng: 0000-0002-1553-1432
Hailin Peng: 0000-0003-1569-0238
Kaihui Liu: 0000-0002-8781-2495

Author Contributions

○These authors contributed equally to this work.

Notes

The authors declare no competing financial interest.

ACKNOWLEDGMENTS

This work was supported by National Key R&D Program of China (2016YFA0300903, 2016YFA0300804, and 2016YFA0200101), NSFC (51522201, 21525310, 91750203, and 11474006), National Equipment Program of China (ZDYZ2015-1), Beijing Graphene Innovation Program (Z161100002116028), the Science, Technology and Innovation Commission of Shenzhen Municipality (ZDSYS20170303165926217, JCYJ20170412152620376), and Guangdong Innovative and Entrepreneurial Research Team Program (2016ZT06D348).

REFERENCES

(1) Stranks, S. D.; Eperon, G. E.; Grancini, G.; Menelaou, C.; Alcocer, M. J. P.; Leijtens, T.; Herz, L. M.; Petrozza, A.; Snaith, H. J. *Science* **2013**, *342*, 341−344.
(2) D'Innocenzo, V.; Grancini, G.; Alcocer, M. J. P.; Kandada, A. R. S.; Stranks, S. D.; Lee, M. M.; Lanzani, G.; Snaith, H. J.; Petrozza, A. *Nat. Commun.* **2014**, *5*, 3586.
(3) Lin, Q. Q.; Armin, A.; Nagiri, R. C. R.; Burn, P. L.; Meredith, P. *Nat. Photonics* **2015**, *9*, 106−112.
(4) Zhou, H. P.; Chen, Q.; Li, G.; Luo, S.; Song, T. B.; Duan, H. S.; Hong, Z. R.; You, J. B.; Liu, Y. S.; Yang, Y. *Science* **2014**, *345*, 542−546.
(5) Ha, S. T.; Liu, X. F.; Zhang, Q.; Giovanni, D.; Sum, T. C.; Xiong, Q. H. *Adv. Opt. Mater.* **2014**, *2*, 838−844.
(6) Dong, Q. F.; Fang, Y. J.; Shao, Y. C.; Mulligan, P.; Qiu, J.; Cao, L.; Huang, J. S. *Science* **2015**, *347*, 967−970.
(7) Shi, D.; Adinolfi, V.; Comin, R.; Yuan, M. J.; Alarousu, E.; Buin, A.; Chen, Y.; Hoogland, S.; Rothenberger, A.; Katsiev, K.; Losovyj, Y.; Zhang, X.; Dowben, P. A.; Mohammed, O. F.; Sargent, E. H.; Bakr, O. M. *Science* **2015**, *347*, 519−522.
(8) Guo, Z.; Wan, Y.; Yang, M. J.; Snaider, J.; Zhu, K.; Huang, L. B. *Science* **2017**, *356*, 59−62.
(9) Tisdale, W. A.; Williams, K. J.; Timp, B. A.; Norris, D. J.; Aydil, E. S.; Zhu, X. Y. *Science* **2010**, *328*, 1543−1547.
(10) Wang, F. J.; Kozawa, D.; Miyauchi, Y.; Hiraoka, K.; Mouri, S.; Ohno, Y.; Matsuda, K. *Nat. Commun.* **2015**, *6*, 6305.
(11) Zhu, H. M.; Miyata, K.; Fu, Y. P.; Wang, J.; Joshi, P. P.; Niesner, D.; Williams, K. W.; Jin, S.; Zhu, X. Y. *Science* **2016**, *353*, 1409−1413.
(12) Li, M. J.; Bhaumik, S.; Goh, T. W.; Kumar, M. S.; Yantara, N.; Gratzel, M.; Mhaisalkar, S.; Mathews, N.; Sum, T. C. *Nat. Commun.* **2017**, *8*, 14350.
(13) Nguyen, D. T.; Lombez, L.; Gibelli, F.; Boyer-Richard, S.; Le Corre, A.; Durand, O.; Guillemoles, J. F. *Nat. Energy* **2018**, *3*, 236−242.
(14) Xing, G. C.; Mathews, N.; Sun, S. Y.; Lim, S. S.; Lam, Y. M.; Gratzel, M.; Mhaisalkar, S.; Sum, T. C. *Science* **2013**, *342*, 344−347.
(15) Wang, L. L.; McCleese, C.; Kovalsky, A.; Zhao, Y. X.; Burda, C. *J. Am. Chem. Soc.* **2014**, *136*, 12205−12208.

DOI: 10.1021/jacs.8b09353
J. Am. Chem. Soc. 2018, 140, 14952−14957

(16) Shen, Q.; Ogomi, Y.; Chang, J.; Tsukamoto, S.; Kukihara, K.; Oshima, T.; Osada, N.; Yoshino, K.; Katayama, K.; Toyoda, T.; Hayase, S. *Phys. Chem. Chem. Phys.* **2014**, *16*, 19984−19992.
(17) Marchioro, A.; Teuscher, J.; Friedrich, D.; Kunst, M.; van de Krol, R.; Moehl, T.; Gratzel, M.; Moser, J. E. *Nat. Photonics* **2014**, *8*, 250−255.
(18) Xing, G. C.; Wu, B.; Chen, S.; Chua, J.; Yantara, N.; Mhaisalkar, S.; Mathews, N.; Sum, T. C. *Small* **2015**, *11*, 3606−3613.
(19) Geim, A. K.; Novoselov, K. S. *Nat. Mater.* **2007**, *6*, 183−191.
(20) Mak, K. F.; Lee, C.; Hone, J.; Shan, J.; Heinz, T. F. *Phys. Rev. Lett.* **2010**, *105*, 136805.
(21) Li, G. H.; Luican, A.; dos Santos, J. M. B. L.; Castro Neto, A. H.; Reina, A.; Kong, J.; Andrei, E. Y. *Nat. Phys.* **2010**, *6*, 109−113.
(22) Liu, K. H.; Zhang, L. M.; Cao, T.; Jin, C. H.; Qiu, D. A.; Zhou, Q.; Zettl, A.; Yang, P. D.; Louie, S. G.; Wang, F. *Nat. Commun.* **2014**, *5*, 4966.
(23) Hong, H.; Liu, C.; Cao, T.; Jin, C. H.; Wang, S. X.; Wang, F.; Liu, K. H. *Adv. Mater. Interfaces* **2017**, *4*, 1601054.
(24) Wang, E. Y.; Lu, X. B.; Ding, S. J.; Yao, W.; Yan, M. Z.; Wan, G. L.; Deng, K.; Wang, S. P.; Chen, G. R.; Ma, L. G.; Jung, J.; Fedorov, A. V.; Zhang, Y. B.; Zhang, G. Y.; Zhou, S. Y. *Nat. Phys.* **2016**, *12*, 1111−1115.
(25) Zhang, Z. W.; Chen, P.; Duan, X. D.; Zang, K. T.; Luo, J.; Duan, X. F. *Science* **2017**, *357*, 788−792.
(26) Yang, T. F.; Zheng, B. Y.; Wang, Z.; Xu, T.; Pan, C.; Zou, J.; Zhang, X. H.; Qi, Z. Y.; Liu, H. J.; Feng, Y. X.; Hu, W. D.; Miao, F.; Sun, L. T.; Duan, X. F.; Pan, A. L. *Nat. Commun.* **2017**, *8*, 1906.
(27) Britnell, L.; Gorbachev, R. V.; Jalil, R.; Belle, B. D.; Schedin, F.; Mishchenko, A.; Georgiou, T.; Katsnelson, M. I.; Eaves, L.; Morozov, S. V.; Peres, N. M. R.; Leist, J.; Geim, A. K.; Novoselov, K. S.; Ponomarenko, L. A. *Science* **2012**, *335*, 947−950.
(28) Lee, C. H.; Lee, G. H.; van der Zande, A. M.; Chen, W. C.; Li, Y. L.; Han, M. Y.; Cui, X.; Arefe, G.; Nuckolls, C.; Heinz, T. F.; Guo, J.; Hone, J.; Kim, P. *Nat. Nanotechnol.* **2014**, *9*, 676−681.
(29) Qiu, C. G.; Zhang, Z. Y.; Xiao, M. M.; Yang, Y. J.; Zhong, D. L.; Peng, L. M. *Science* **2017**, *355*, 271−276.
(30) Pomerantseva, E.; Gogotsi, Y. *Nat. Energy* **2017**, *2*, 17089.
(31) Castro Neto, A. H.; Guinea, F.; Peres, N. M. R.; Novoselov, K. S.; Geim, A. K. *Rev. Mod. Phys.* **2009**, *81*, 109−162.
(32) Qiu, C.; Liu, F.; Xu, L.; Deng, B.; Xiao, M.; Si, J.; Lin, L.; Zhang, Z.; Wang, J.; Guo, H. *Science* **2018**, *361*, 387.
(33) He, J. Q.; Kumar, N.; Bellus, M. Z.; Chiu, H. Y.; He, D. W.; Wang, Y. S.; Zhao, H. *Nat. Commun.* **2014**, *5*, 5622.
(34) Massicotte, M.; Schmidt, P.; Vialla, F.; Schadler, K. G.; Reserbat-Plantey, A.; Watanabe, K.; Taniguchi, T.; Tielrooij, K. J.; Koppens, F. H. L. *Nat. Nanotechnol.* **2016**, *11*, 42−46.
(35) Yu, W. J.; Liu, Y.; Zhou, H. L.; Yin, A. X.; Li, Z.; Huang, Y.; Duan, X. F. *Nat. Nanotechnol.* **2013**, *8*, 952−958.
(36) Britnell, L.; Ribeiro, R. M.; Eckmann, A.; Jalil, R.; Belle, B. D.; Mishchenko, A.; Kim, Y. J.; Gorbachev, R. V.; Georgiou, T.; Morozov, S. V.; Grigorenko, A. N.; Geim, A. K.; Casiraghi, C.; Castro Neto, A. H.; Novoselov, K. S. *Science* **2013**, *340*, 1311−1314.
(37) Lee, Y.; Kwon, J.; Hwang, E.; Ra, C. H.; Yoo, W. J.; Ahn, J. H.; Park, J. H.; Cho, J. H. *Adv. Mater.* **2015**, *27*, 41−46.
(38) Wang, Y. S.; Zhang, Y. P.; Lu, Y.; Xu, W. D.; Mu, H. R.; Chen, C. Y.; Qiao, H.; Song, J. C.; Li, S. J.; Sun, B. Q.; Cheng, Y. B.; Bao, Q. L. *Adv. Opt. Mater.* **2015**, *3*, 1389−1396.
(39) Wang, J. T. W.; Ball, J. M.; Barea, E. M.; Abate, A.; Alexander-Webber, J. A.; Huang, J.; Saliba, M.; Mora-Sero, I.; Bisquert, J.; Snaith, H. J.; Nicholas, R. J. *Nano Lett.* **2014**, *14*, 724−730.
(40) Yan, K. Y.; Wei, Z. H.; Li, J. K.; Chen, H. N.; Yi, Y.; Zheng, X. L.; Long, X.; Wang, Z. L.; Wang, J. N.; Xu, J. B.; Yang, S. H. *Small* **2015**, *11*, 2269−2274.
(41) Dou, L. T.; Wong, A. B.; Yu, Y.; Lai, M. L.; Kornienko, N.; Eaton, S. W.; Fu, A.; Bischak, C. G.; Ma, J.; Ding, T. N.; Ginsberg, N. S.; Wang, L. W.; Alivisatos, A. P.; Yang, P. D. *Science* **2015**, *349*, 1518−1521.
(42) Zhang, J. C.; Lin, L.; Sun, L. Z.; Huang, Y. C.; Koh, A. L.; Dang, W. H.; Yin, J. B.; Wang, M. Z.; Tan, C. W.; Li, T. R.; Tan, Z. J.; Liu, Z. F.; Peng, H. L. *Adv. Mater.* **2017**, *29*, 1700639.
(43) Lee, J. E.; Ahn, G.; Shim, J.; Lee, Y. S.; Ryu, S. *Nat. Commun.* **2012**, *3*, 1024.
(44) Hong, X. P.; Kim, J.; Shi, S. F.; Zhang, Y.; Jin, C. H.; Sun, Y. H.; Tongay, S.; Wu, J. Q.; Zhang, Y. F.; Wang, F. *Nat. Nanotechnol.* **2014**, *9*, 682−686.
(45) Ji, Z. H.; Hong, H.; Zhang, J.; Zhang, Q.; Huang, W.; Cao, T.; Qiao, R. X.; Liu, C.; Liang, J.; Jin, C. H.; Jiao, L. Y.; Shi, K. B.; Meng, S.; Liu, K. H. *ACS Nano* **2017**, *11*, 12020−12026.
(46) Blancon, J.-C.; Tsai, H.; Nie, W.; Stoumpos, C. C.; Pedesseau, L.; Katan, C.; Kepenekian, M.; Soe, C. M. M.; Appavoo, K.; Sfeir, M. Y. *Science* **2017**, *355*, 1288−1292.
(47) Breusing, M.; Ropers, C.; Elsaesser, T. *Phys. Rev. Lett.* **2009**, *102*, 086809.
(48) Tully, J. C. *J. Chem. Phys.* **1990**, *93*, 1061−1071.
(49) Craig, C. F.; Duncan, W. R.; Prezhdo, O. V. *Phys. Rev. Lett.* **2005**, *95*, 163001.
(50) Wang, H.; Bang, J.; Sun, Y. Y.; Liang, L. B.; West, D.; Meunier, V.; Zhang, S. B. *Nat. Commun.* **2016**, *7*, 11504.
(51) Smith, I. C.; Hoke, E. T.; Solis-Ibarra, D.; McGehee, M. D.; Karunadasa, H. I. *Angew. Chem., Int. Ed.* **2014**, *53*, 11232−11235.
(52) Tsai, H. H.; Nie, W. Y.; Blancon, J. C.; Toumpos, C. C. S.; Asadpour, R.; Harutyunyan, B.; Neukirch, A. J.; Verduzco, R.; Crochet, J. J.; Tretiak, S.; Pedesseau, L.; Even, J.; Alam, M. A.; Gupta, G.; Lou, J.; Ajayan, P. M.; Bedzyk, M. J.; Kanatzidis, M. G.; Mohite, A. D. *Nature* **2016**, *536*, 312−316.
(53) Leng, K.; Abdelwahab, I.; Verzhbitskiy, I.; Telychko, M.; Chu, L. Q.; Fu, W.; Chi, X.; Guo, N.; Chen, Z. H.; Chen, Z. X.; Zhang, C.; Xu, Q. H.; Lu, J.; Chhowalla, M.; Eda, G.; Loh, K. P. *Nat. Mater.* **2018**, *17*, 908−914.
(54) Zhang, Y. B.; Tan, Y. W.; Stormer, H. L.; Kim, P. *Nature* **2005**, *438*, 201−204.
(55) Wang, F.; Zhang, Y. B.; Tian, C. S.; Girit, C.; Zettl, A.; Crommie, M.; Shen, Y. R. *Science* **2008**, *320*, 206−209.
(56) Wehling, T. O.; Novoselov, K. S.; Morozov, S. V.; Vdovin, E. E.; Katsnelson, M. I.; Geim, A. K.; Lichtenstein, A. I. *Nano Lett.* **2008**, *8*, 173−177.
(57) Balog, R.; Jorgensen, B.; Nilsson, L.; Andersen, M.; Rienks, E.; Bianchi, M.; Fanetti, M.; Laegsgaard, E.; Baraldi, A.; Lizzit, S.; Sljivancanin, Z.; Besenbacher, F.; Hammer, B.; Pedersen, T. G.; Hofmann, P.; Hornekaer, L. *Nat. Mater.* **2010**, *9*, 315−319.
(58) Xu, X. Z.; Zhang, Z. H.; Dong, J. C.; Yi, D.; Niu, J. J.; Wu, M. H.; Lin, L.; Yin, R. K.; Li, M. Q.; Zhou, J. Y.; Wang, S. X.; Sun, J. L.; Duan, X. J.; Gao, P.; Jiang, Y.; Wu, X. S.; Peng, H. L.; Ruoff, R. S.; Liu, Z. F.; Yu, D. P.; Wang, E. G.; Ding, F.; Liu, K. H. *Sci. Bull.* **2017**, *62*, 1074−1080.
(59) Zhang, Z. K.; Du, J. H.; Zhang, D. D.; Sun, H. D.; Yin, L. C.; Ma, L. P.; Chen, J. S.; Ma, D. G.; Cheng, H. M.; Ren, W. C. *Nat. Commun.* **2017**, *8*, 14560.

DOI: 10.1021/jacs.8b09353
J. Am. Chem. Soc. 2018, 140, 14952−14957